# Time-Dependent Density Functional Theory Studies of the Photoswitching of the Two-Photon Absorption Spectra in Stilbene, Metacyclophenadiene, and Diarylethene Chromophores

**Aurora E. Clark**[†]

*Department of Chemistry, Washington State University, Pullman, Washington 99164*

*Received: November 28, 2005; In Final Form: January 20, 2006*

Photochromophores such as *cis*-stilbene (**1a**), metacyclophenadiene (**2a**), and the diarylethene **3a** undergo photoinduced conrotatory opening and closing of a central bond and are currently being sought out as potential candidates for media within 3D optical information storage devices. Strong molecular two-photon absorption (inducing the reversible photoisomerization) is a necessary feature for this application due to the need for high 3D spatial resolution. Here, the one- and two-photon absorption (OPA and TPA) characteristics of the open- and closed-ring isomers of **1**−**3** have been investigated using time-dependent density functional theory. It was determined that the excited states populated by two-photon absorption were nearly 1 eV higher in energy than the lowest energy excited state populated by one-photon absorption. The electronic structures of the TPA and OPA accessed states were then compared utilizing natural transition orbital analysis. There, it was found that states excited by OPA had $\pi\pi^*$ character about the C−C framework associated with the bond formation/scission of the central C−C bond. In contrast, the states populated by TPA have $\pi\pi^*$ character along the C−C skeletal periphery, including phenyl excitations. It is postulated that these differences in excited state electronic structure may lead to reaction pathways alternative to photoisomerization about the central C−C bond, impacting the utility of these compounds as 3D information storage media.

## Introduction

Current optical data storage techniques have fundamental limitations in the available memory density owing to their 2-dimensional nature and the use of diffraction limited laser burn (heat-mode) recording. The latter constraint may be overcome by photon-mode recording, where the storage medium undergoes a reversible photoinduced isomerization (photochromism). Memory can also be stored within the 3D volume of the material, increasing the data holding capacity by a factor proportional to the thickness of the medium. Within this theme, the two-photon absorption (TPA) of photochromic compounds can be utilized to achieve higher spatial resolution than one-photon absorption (OPA). Thus, it is desirable to combine the photon-mode recording abilities of photochromophores with their TPA characteristics to generate high-density multilayer storage devices.

The *cis*-stilbene (**1a**) to dihydrophenanthrene (**1b**) conversion (Scheme 1) represents one of the most general photochromic processes, involving the photoinduced conrotatory opening and closing of a central bond. Chemically robust systems based upon the stilbene architecture have subsequently been synthesized, including metacyclophenadiene (**2a**), which is converted to dihydropyrene (**2b**), as well as bisbenzothienylethene (**3a**) and its ring-closed isomer **3b**. In each case, the open-ring and closed-ring isomers exhibit markedly different physical properties (e.g., absorption spectra) that derive from altering the $\pi$-conjugation as a function of irradiation. The diarylethenes (**3a** and **3b**) are particularly relevant for optical 3D storage media, as they fulfill the requirements needed for materials applications, namely, thermal stability and resistance to linear optical photofatigue. As such, much effort has been dedicated to understanding the photophysics associated with diarylethenes, including spectroscopic studies[1−10] and the optimization of one-photon absorption quantum yield and minimization of photofatigue via synthetic strategies.[1−5,11−17] Previous theoretical studies on photochromophores akin to those in Scheme 1 have focused upon understanding the one-photon induced excited state isomerization potential energy surfaces, which are complex and in the case of dithienylethene can involve a stepwise multiphoton mechanism and a conical intersection between states.[18−20]

The nonlinear optical characteristics of photochromophores have been widely studied, though much of this effort has been dedicated to examining the first hyperpolarizability, $\beta$, with an aim toward the design of systems with large second-harmonic generation. In this respect, the diarylethenes have exhibited a reversible alteration of $\beta$ from high to low response as a function of the isomeric form (photoswitching).[16,21,22] In contrast, the two-photon absorption and its frequency dependent cross section, $\sigma_{TPA}$, are related to the imaginary part of the frequency dependent second hyperpolarizability, $\gamma$, which remains an unexamined, but highly relevant, aspect of the photophysical properties of photochromic systems.

In this article, we investigate two-photon absorption as a function of isomeric form for systems **1**−**3**, using the recently developed methodology of Tretiak and co-workers based upon time-dependent density functional theory (TDDFT).[23] Our results illustrate that photoswitching of the TPA can be much more dramatic than the one-photon process, with a significant absorbance in one isomer and no nonlinear response in another. Necessarily, this highlights the significant synthetic tunability of TPA properties. However, from the perspective of 3D information storage, the potential reactivity of excited states

[†] E-mail: auclark@wsu.edu.

10.1021/jp056904u CCC: $33.50 
Published on Web 02/18/2006

**SCHEME 1**

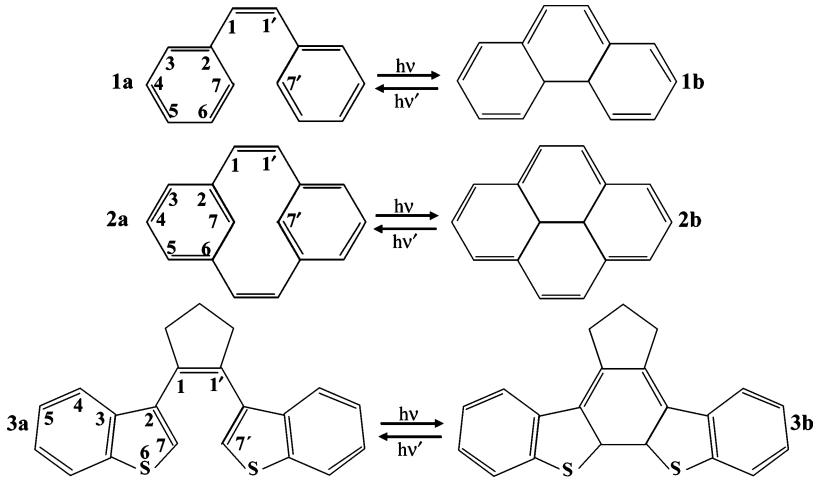


accessed by two-photon absorption is more pertinent. Here, natural transition orbital analysis indicates that TPA excited states have electronic structures that are significantly different from those excited by OPA, which may alter the excited state energetics for photocyclization or lead to competitive alternative photochemical pathways. These results illustrate the need for detailed theoretical examination of the potential energy surfaces associated with reactivity induced by two-photon absorption (in progress) in addition to experimental studies of the product distributions that result from such excitations.

## Theoretical Methods

The geometries of **1a**−**3b** were optimized using DFT with the B3LYP combination of exchange and correlation functionals[24,25] and the 6-31G* basis set,[26−28] as implemented in the Gaussian03 quantum chemistry code.[29] The optical properties were examined using TDDFT, which provides a description of an excited state in terms of all possible single excitations from occupied to virtual orbitals. For a given state, the most important of these "amplitudes" are given in terms of the pair of orbitals involved in the excitation and the relative percent contribution of each excitation. In typical cases there are several contributors to a given state in the TDDFT results. One can clarify the interpretation by employing a natural transition orbital (NTO) analysis, which provides the most compact description of the state by a rotation of the occupied and virtual orbitals that diagonalizes the transition density matrix connecting the ground and excited states.[30,31] In most cases the overall description reduces to a single configuration of "hole" and "particle" NTOs for a given state. The fraction of the total transition density that can be recovered by a particular hole−particle pair is given by its eigenvalue. Excited states populated by one- and two-photon absorption, as well as the NTOs, were subsequently determined with the same functionals and basis set and at the optimized ground state geometry using the development version of Gaussian98.[32] The second hyperpolarizability, $\gamma$, as well as the frequency-dependent TPA cross section, $\sigma_{TPA}$, and the resulting spectra were calculated utilizing 12 excited states and line widths of 0.1 eV with the method recently reported by Tretiak and co-workers.[23] There, a density matrix formulation of the time-dependent Kohn−Sham equations is used to obtain expressions for the frequency-dependent optical polarizabilities, which are then used to compute the third-order optical response (second-order nonlinear response) and, as a result, $\gamma$ and $\sigma_{TPA}$ as a function of frequency. Both the method and basis set utilized in this study have been shown to yield errors that are comparable to the best available literature results for a similar series of extended conjugated systems.[23]

## Results and Discussion

**Geometries and One-Photon Excitations.** The optimized structural parameters for the $C_2$ geometry of **1a** and **1b**, presented in Table 1, are in good agreement with previous studies.[33−35] DFT predicts that **1b** is less stable than **1a** by 38.9 kcal/mol, in comparison to previous semiempirical MNDO calculations which place **1b** > **1a** by 27.3 kcal/mol.[36] Increasing the basis set size to 6-311+G(d,p) did not significantly alter either geometry or stabilization energy. Photocyclization most notably results in an increase in planarity and enhanced $\pi$-electron delocalization, which is manifested as a red shift in the one-photon absorption. In the case of **1a**, TDDFT predicts the lowest energy transition to be HOMO → LUMO, populating the $1^1$B state at 301.5 nm (4.11 eV). The $1^1$B state is believed to be the initiating state for photoinduced ring closure as it has delocalized $\pi\pi^*$ character about the bridging ethyl unit. The calculated excitation energy is well within the experimental absorbance range of **1a**, between 290 and 310 nm.[37] The natural transition orbitals (NTOs) for the $1^1$B state of **1a** are presented in Figure 1. Here, the NTOs are nearly identical to the HOMO and LUMO, clearly showing the reorganization of the $\pi$ system that leads to photoisomerization. Photoinduced ring opening of **1b** to form **1a** is similarly believed to occur by HOMO → LUMO excitation to the $1^1$B state. TDDFT predicts the transition to occur at much lower energy than in the open-ring isomer (506.3 nm, 2.45 eV) due to enhanced $\pi$-delocalization (Table 2). The calculated excitation energy is slightly lower than the experimentally observed absorption at ∼450 nm.[34,38] The NTO particle orbital associated with the transition clearly shows $\pi$ bonding character along the bridging ethyl moiety and an antibonding interaction between C7 and C7′, facilitating ring scission (Figure 1).

The second photochromic system of interest is represented by the reversible metacyclophenadiene (**2a**) to dihydropyrene (**2b**) conversion (Scheme 1). The computed $C_{2h}$ structures of **2a** and **2b** are in good agreement with the experimental structures of the methylated derivatives, **2a′**−**2b′** (Table 1).[39] The TDDFT OPA properties are similar between **2a** and *cis*-stilbene, with the lowest energy transition of **2a** occurring at 296.6 nm (4.18 eV), populating the $2^1B_u$ state, and involving the HOMO−1 and LUMO+1 orbitals. This state is analogous to the $1^1$B state of *cis*-stilbene as seen by the hole and particle NTOs in Figure 1 and likely leads to ring closure.

**TABLE 1: B3LYP/6-31G* Optimized Geometries of 1a−3b**[a]

| $E$ | $E_{ZPE}^{298}$ | $r_{7,7'}$ | $r_{1,1'}$ | $r_{1,2}$ | $r_{2,3}$ | $r_{3,4}$ | $\alpha_{1',1,2}$ | $\alpha_{1,2,7}$ | $\alpha_{7,2,3}$ | $\alpha_{2,7,6}$ | $\omega_{1',1,2,7}$ |
|---|---|---|---|---|---|---|---|---|---|---|---|
| | | | | | **1a** ($C_2$) | | | | | | |
| −540.701 968 9 | −540.259 517 9 | 3.245 | 1.350 | 1.475 | 1.407 | 1.394 | 131.28 | 123.24 | 117.96 | 120.82 | 33.31 |
| | | | | | **1b** ($C_2$) | | | | | | |
| −540.638 755 8 | −540.198 041 8 | 1.543 | 1.432 | 1.366 | 1.441 | 1.359 | 121.84 | 119.38 | 118.13 | 112.04 | 5.26 |
| | | | | | **2a** ($C_2h$) | | | | | | |
| −616.854 319 | −616.386 698 9 | 2.598 | 1.358 | 1.479 | 1.406 | 1.397 | 126.70 | 120.67 | 117.76 | 120.83 | 35.20 |
| | | (2.57) | (1.34) | (1.48) | (1.40) | (1.38) | (126.0) | (121.3) | (117.7) | (119.9) | |
| | | | | | **2b** ($C_2h$) | | | | | | |
| −616.887 135 1 | −616.419 493 1 | 1.523 | 1.397 | 1.402 | 1.345 | 1.400 | 122.04 | 117.09 | 118.25 | 115.09 | 6.54 |
| | | (1.53) | (1.39) | (1.39) | (1.39) | (1.39) | (122.3) | (116.8) | (118.1) | (114.3) | (9.2) |
| | | | | | **3a** ($C_1$) | | | | | | |
| −1 606.251 5105 | −1 605.617 953 5 | 4.115 | 1.355 | 1.473 | 1.457 | 1.409 | 127.06 | 122.57 | 111.33 | 114.43 | 44.24 |
| | | | | | **3b** ($C_1$) | | | | | | |
| −1 606.255 526 7 | −1 605.619 418 7 | 1.515 | 1.465 | 1.360 | 1.458 | 1.410 | 121.27 | 116.73 | 111.76 | 106.89 | 8.00 |

[a] Distance in Å, angles in degrees, energy in hartrees. The definitions of bond lengths and angles follow the numbering system outlines in Scheme 1. Experimental X-ray structural parameters are presented in parentheses.[39] The total electronic energy, $E$, and the energy after zero point and thermal corrections, $E_{ZPE}$,[298] are given.

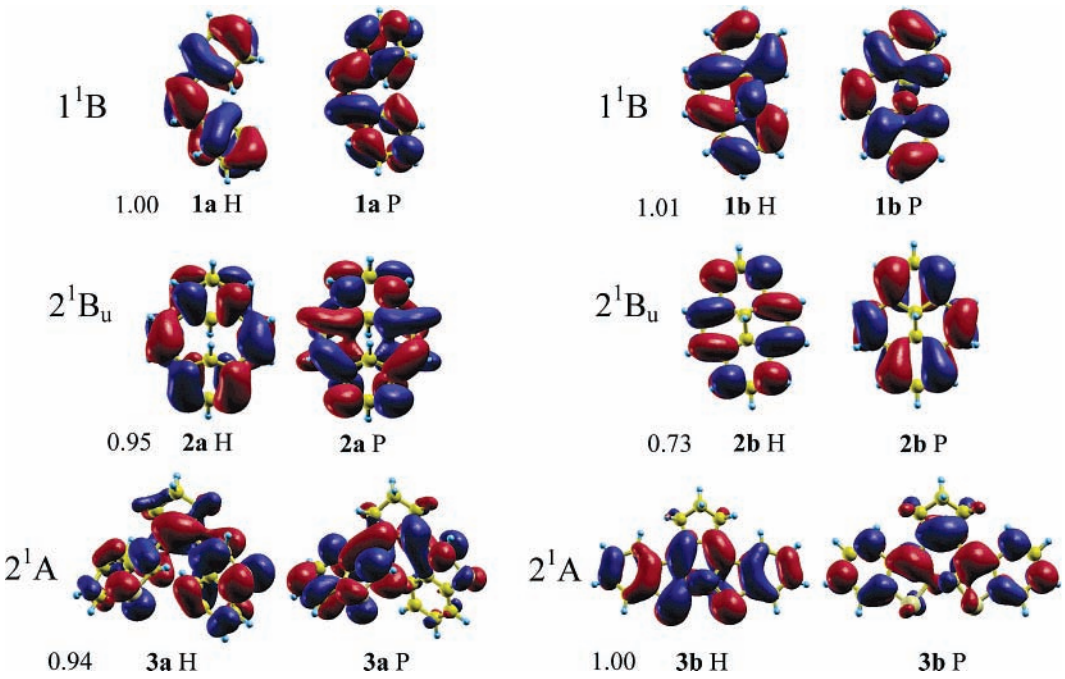


**Figure 1.** Hole (H) and particle (P) natural transition orbitals (NTOs), as well as their coefficients, that are involved in the lowest energy transitions with appreciable oscillator strength for **1a**−**3b**, using TDDFT. The NTO coefficients represent the extent to which the excitation can be written as a single configuration.

Experimentally, **2a′** absorbs at wavelengths less than 313 nm, in agreement with the TDDFT results for the nonmethylated derivative.[40] The optical properties of closed-ring isomer **2b** are somewhat different from those of dihydrophenanthrene **1b**, particularly with regard to the nature of the TDDFT "wave function" of the lowest energy optically allowed excited state, $2^1A_u$, which is populated by excitation at 355.0 nm ($\lambda_{exp}$ **2b′** = 365 nm).[41] The $2^1A_u$ state (3.49 eV) is composed of two dominant configurations, one HOMO → LUMO+1, and the second HOMO−1 → LUMO. NTO analysis does not reduce the number of configurations, indicating that the $2^1A_u$ state is truly multiconfigurational in character. Although excitation to the $2^1A_u$ state has an oscillator strength (*f*) of 0.3, a much stronger excitation ($f = 0.9$) is predicted at 311.6 nm (3.98 eV) to the $2^1B_u$ state. The latter is described predominantly by a HOMO−1 → LUMO+1 configuration that is more similar to the first excited states of **1b**, as illustrated by the natural transition orbitals shown in Figure 1. It is therefore likely that photoisomerization of **2b** is initiated by population of the $2^1B_u$ state.

Experimentally, it has been shown that the dimethyl derivative of metacyclophenadiene, **2a′**, is less stable than its closed-ring counterpart, **2b′**, by 2.5 kcal/mol.[40] However, our DFT study of the non-methyl analogues predicts this gap to be much larger at 20.4 kcal/mol. Further investigation shows that the discrepancy between the DFT and experimentally determined values is not due to an inappropriately small basis (increasing to *cc*-PVTZ does not significantly alter the stabilization energy) and is reproducible using more correlated computational techniques. Starting with semiempirical methods, previous AM1 calculations find **2b** < **2a** by ∼8 kcal/mol,[42] while SCF/MM2 calculations incorrectly predict **2a′** < **2b′** by 13 kcal/mol.[43] These results prompted us to perform single point Hartree−Fock, second-order Møller−Plesset perturbation theory (MP2), and coupled-

**TABLE 2: TDDFT Results for the Lowest Energy Excited States of 1a−3b[a]**

| state | configuration | % | *E* (nm) | *E* (eV) | *f* |
|---|---|---|---|---|---|
| | | **1a** ($C_2$) | | | |
| $1^1$B | HOMO → LUMO | 82.99 | 301.5 | 4.11 | 0.4 |
| $3^1$B | HOMO−1 → LUMO | 38.81 | 238.9 | 5.19 | 0.2 |
| | HOMO → LUMO+1 | 44.96 | | | |
| $5^1$A | HOMO → LUMO+3 | 45.07 | 215.8 | 5.75 | 0.1 |
| | HOMO−3 → LUMO | 21.04 | | | |
| | | **1b** ($C_2$) | | | |
| $1^1$B | HOMO → LUMO | 74.38 | 506.3 | 2.45 | 0.2 |
| $3^1$A | HOMO−1 → LUMO | 33.80 | 310.7 | 3.99 | 0.2 |
| | HOMO → LUMO+1 | 38.47 | | | |
| $4^1$B | HOMO−2 → LUMO+2 | 46.70 | 237.0 | 5.23 | 0.3 |
| $5^1$B | HOMO−5 → LUMO | 89.46 | 218.5 | 5.67 | 0.1 |
| | | **2a** ($C_2h$) | | | |
| $2^1B_u$ | HOMO−1 → LUMO+1 | 81.92 | 296.6 | 4.18 | 0.3 |
| $3^1B_u$ | HOMO−4 → LUMO | 74.42 | 229.5 | 5.40 | 0.1 |
| | | **2b** ($C_2h$) | | | |
| $2^1A_u$ | HOMO → LUMO+1 | 25.92 | 355.0 | 3.49 | 0.3 |
| | HOMO−1 → LUMO | 38.72 | | | |
| $2^1B_u$ | HOMO−1 → LUMO+1 | 46.08 | 311.6 | 3.98 | 0.9 |
| | HOMO → LUMO | 13.52 | | | |
| | | **3a** ($C_1$) | | | |
| $2^1$A | HOMO → LUMO | 80.20 | 304.3 | 4.07 | 0.1 |
| $3^1$A | HOMO → LUMO+1 | 77.75 | 301.4 | 4.11 | 0.1 |
| $4^1$A | HOMO−1 → LUMO | 74.63 | 274.6 | 4.52 | 0.1 |
| | | **3b** ($C_1$) | | | |
| $2^1$A | HOMO → LUMO | 80.57 | 447.3 | 2.77 | 0.3 |
| $4^1$A | HOMO−2 → LUMO | 84.45 | 330.0 | 3.76 | 0.2 |
| $7^1$A | HOMO−1 → LUMO+3 | 81.72 | 288.1 | 4.30 | 0.1 |

[a] *f* is the oscillator strength, the configuration represents the orbitals involved in the transition, and the % is the contribution of the configuration to the state.

cluster calculations with single, double, and triple excitations [CCSD(T)] (all electrons correlated) for **2a** and **2b** at the DFT optimized geometries with the 6-31G* basis set. Based upon these calculations, HF theory favors **2b** by 4.0 kcal/mol, MP2 predicts **2b** < **2a** by 24.1 kcal/mol, and CCSD determines **2b** < **2a** by 14.5 kcal/mol. As the DFT geometries are quite similar to the experimental X-ray structures, it is not anticipated that geometry optimization by the more highly correlated methods would lead to significant differences in these predicted stabilization energies. Indeed, geometry optimization of **2a** and **2b** using MP2 leads to a stabilization energy of 23.7 kcal/mol, which is nearly that derived from the single point calculations. It is then apparent that there is a substantial discrepancy between the theoretical and experimental values, which does not disappear with basis set expansion or increased electron correlation in the computational method.

In the last system, photoswitching of a 1,2-bis(2-methyl-1-benzothiophen-3-yl) perfluorocyclopentene (MBP) derivative is examined, where the internal methyl groups as well as the fluorine atoms have been replaced with hydrogen. In general, there is excellent agreement with the $C_1$ structural parameters of the open-ring model, **3a**, and MBP; however, replacement of the internal methyl units with H atoms decreases the steric interaction between the internal carbons and leads to shortening of $r_{C7C7'}$ by ∼0.6 Å (Table 1).[44,45] TDDFT predicts that the lowest energy excited state of **3a** ($2^1$A) derives from a HOMO → LUMO transition at 304.3 nm (4.07 eV). Close in energy is the $3^1$A state which is populated by excitation from the HOMO to the LUMO+1. Both states are within the energy range of absorption for a variety of substituted thienylethenes.[46] The NTOs for the lower energy transition appear in Figure 1 and are similar to those observed for **1a**−**2a**. Photoinduced ring closure of **3a** results in the product **3b**, which is 2.8 kcal/mol lower in energy, possessing a nearly planar $C_1$ structure. This isomer exhibits an ∼150 nm shift in the lowest energy transition (HOMO → LUMO) at 447.3 nm (2.77 eV), as well as a 3-fold increase in oscillator strength relative to **3a**. The resulting $2^1$A state is characterized by a single configuration involving the NTOs shown in Figure 1.

**TABLE 3: TDDFT Results for the Higher Energy Excited States of 1a−3b Populated by TPA[a]**

| state | configuration | % | *E* (nm) | *E* (eV) | $f_{OPA}$ | $\sigma_{TPA}$ | $\lambda_{TPA}$ |
|---|---|---|---|---|---|---|---|
| | | **1a** ($C_2$) | | | | | |
| $2^1$A | HOMO−3 → LUMO | 61.0 | 243.2 | 5.10 | 0.00 | 284.1 | 486.3 |
| | HOMO → LUMO+3 | 36.7 | | | | | |
| | | **1b** ($C_2$) | | | | | |
| $2^1$A | HOMO−1 → LUMO | 53.3 | 374.7 | 3.31 | 0.00 | 461.5 | 747.8 |
| | HOMO → LUMO+1 | 49.1 | | | | | |
| | | **2a** ($C_2$h) | | | | | |
| $2^1A_g$ | HOMO−2 → LUMO+1 | 41.0 | 247.4 | 5.01 | 0.00 | 194.2 | 492.8 |
| | HOMO−1 → LUMO+2 | 48.7 | | | | | |
| | | **3b** ($C_1$) | | | | | |
| $4^1$A | HOMO → LUMO+1 | 53.8 | 304.5 | 4.07 | 0.01 | 358.9 | 609.4 |
| | HOMO → LUMO+4 | 24.4 | | | | | |
| | HOMO → LUMO+3 | 10.9 | | | | | |
| $5^1$A | HOMO → LUMO+3 | 44.7 | 297.0 | 4.17 | 0.00 | 607.5 | 597.2 |
| | HOMO → LUMO+1 | 20.6 | | | | | |
| | HOMO−3 → LUMO | 14.5 | | | | | |
| $7^1$A | HOMO → LUMO+3 | 32.4 | 276.2 | 4.49 | 0.06 | 188.5 | 554.8 |
| | HOMO → LUMO+2 | 48.9 | | | | | |

[a] *f* is the one-photon absorption oscillator strength, the configuration represents the orbitals involved in the analogous OPA transition, the % is the contribution of the configuration to that excited state, $\sigma_{TPA}$ is the two-photon absorption cross section, and $\lambda_{TPA}$ is the position of the TPA maxima.

**Two-Photon Absorption.** As a nonlinear optical response, two-photon absorption is related to the second-order hyperpolarizability, $\gamma$, also known as the third-order polarizability. The selection rules associated with TPA mandate that its cross section, $\sigma_{TPA}$, is highly dependent upon the molecular geometry and that parity will forbid TPA to an OPA state in centrosymmetric molecules such as **1** and **2**. Previous studies have additionally shown that structural parameters such as bond-length alternation and planarity are expected to affect the strength of TPA transitions.[23] In the case of *cis*-stilbene, each phenyl ring is canted by 33.3° relative to the plane of the ethylene unit and a bond-length alternative C−C periphery is observed, indicating less $\pi$ conjugation than its planar, closed-ring, counterpart **1b**. In general, TPA cross sections ($\sigma_{TPA}$) increase with enhanced $\pi$ conjugation, and thus it is anticipated that nonplanarity of **1a** should lead to a small $\sigma_{TPA}$ for allowed transitions ($\sigma_{TPA}$ < 100 Göppert-Mayers, 1 GM = $10^{-50}$ cm$^4$ s). Indeed, TDDFT predicts five TPA resonances, four of which have cross section values below 100 GM (Table 3, Figure 2). One exception is observed at 486.3 nm with $\sigma_{TPA}$ = 284.1 GM, facilitating population of the $2^1$A excited state (5.09 eV above the $1^1$A ground state). Recall that excitation to the $2^1$A state exhibited no oscillator strength within the linear regime and is nearly 1 eV higher in energy than the $1^1$B state that is populated by OPA. In comparison to *cis*-stilbene, **1b** exhibits more intense two-photon absorption owing to increased $\pi$ delocalization, which is reflected in the non bond length alternative C−C periphery and near planar geometry. Here, a single resonance is observed at 747.8 nm, with a $\sigma_{TPA}$ value of 461.5 GM, exciting **1b** to the $2^1$A state (Figure 2, Table 3). The $2^1$A state exhibited no oscillator strength for one-photon absorption, lying

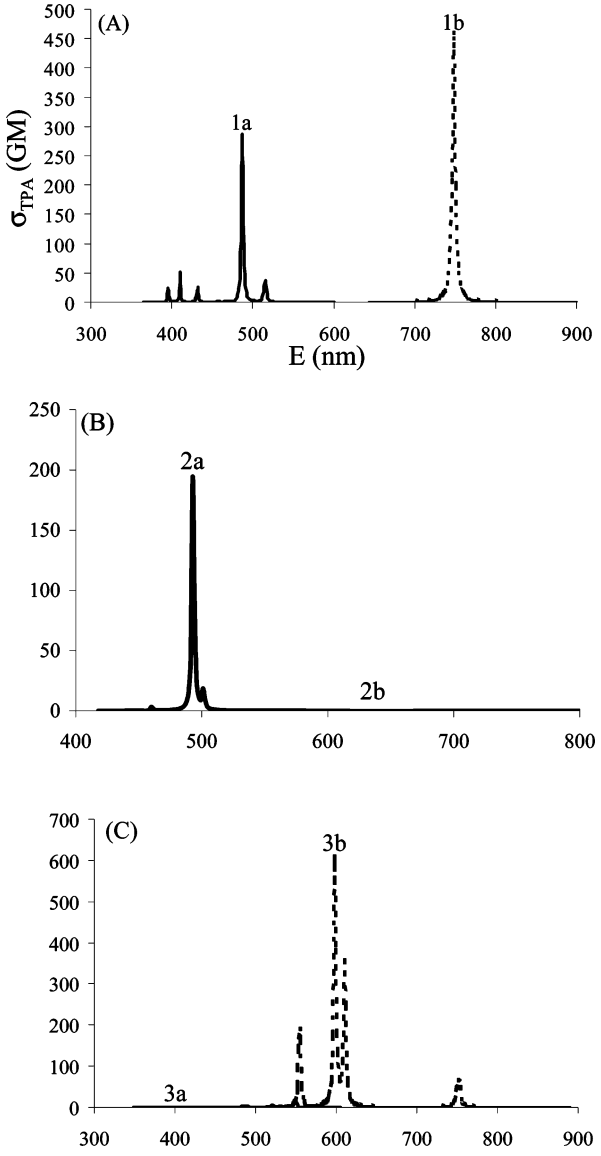


**Figure 2.** Two photon absorption cross sections, $\sigma_{TPA}$ (in GM, 1 GM $= 10^{-50}$ cm$^4$/s), as a function of wavelength (nm) for **1a**−**1b** (A), **2a**−**2b** (B), and **3a**−**3b** (C) calculated from TDDFT (utilizing 12 excited states) and using the method described in ref 23, with a 0.1 eV line width.

3.31 eV above the ground state and 0.86 eV above the lowest energy excited state.

Given the high energy of the states populated by TPA, it is feasible that their electronic structures, and hence reactivity, may differ significantly from the low-energy states accessed by a single-photon process. A detailed investigation into the respective photoisomerization potential energy surfaces is beyond the scope of this work and will be the topic of future study. However, the electronic structures of both high- and low-energy states can be compared by examination of their respective NTOs. In *cis*-stilbene, the OPA state that is believed to be responsible for photocyclization, $1^1$B, has a TDDFT "wave function" that is characterized by a single configuration, representing a delocalized $\pi\pi^*$ transition across both the ethyl and phenyl units (Table 2, Figure 1). In contrast, the $2^1$A state that is excited by TPA has a TDDFT "wave function" that is multiconfigurational in nature, and whose NTOs portray a localized $\pi\pi^*$ transition on the phenyl groups (Table 3, Figure 3). Photoisomerization from dihydrophenanthrene (**1b**) to *cis*-stilbene (**1a**) via OPA is similarly characterized by a single-configuration excited state,

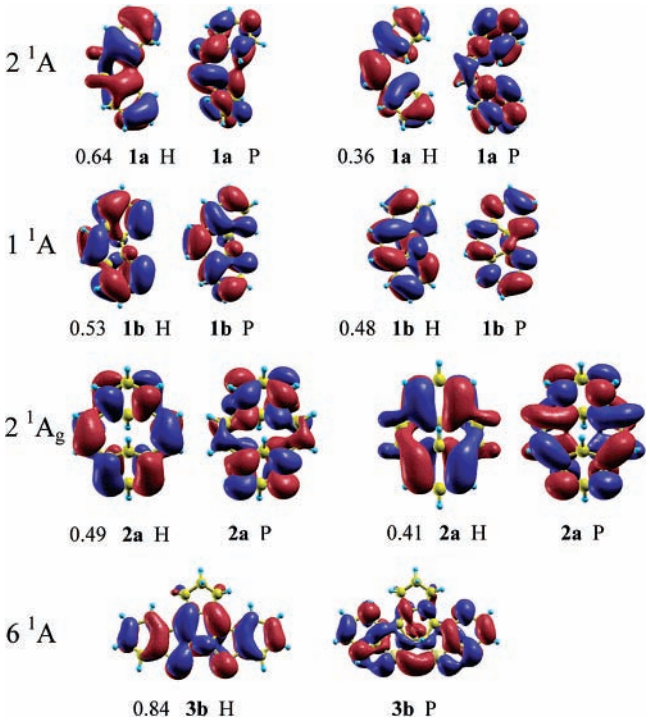


**Figure 3.** Hole (H) and particle (P) natural transition orbitals (NTOs), as well as their coefficients, that are involved in the excited states populated by two-photon absorption by **1a**−**3b** using TDDFT. The NTO coefficients represent the extent to which the excitation can be written as a single configuration.

$1^1$B, whose NTOs depict $\pi\pi^*$ excitation about the C1−C2 and C1′−C2′ double bonds. In contrast, the NTOs for the high-energy $2^1$A state that is populated by the two-photon process are primarily $\pi\pi^*$ in character, but again localized on the phenyl periphery. Thus, the high-energy excited states that are associated with two-photon absorption exhibit excitation on the C2−C7 and C2′−C7′ rings rather than the C2−C1−C1′−C2′ skeletal core.

A similar description of the excited state electronic structure emerges for the metacyclophenadiene and diarylethene systems. However, in these cases only one isomer exhibits a nonlinear optical response. In particular, **2a** is predicted to have a modest TPA at 492.8 nm to the $2^1A_g$ state (2.52 eV above the ground state), while its closed-ring isomer does not. Natural transition orbital analysis of the $2^1A_g$ state of **2a** reveals two sets of hole and particle orbitals, each of which contributes ∼50% to the overall excitation. Both sets of NTOs exhibit $\pi\pi^*$ character on the phenyl periphery, with no excitation on the ethyl bridge. In the diarylethene system, it is the closed-ring isomer, **3b**, which has significant two-photon absorption, while the open-ring isomer has no response. Indeed **3b** demonstrates the most intense two-photon absorption within the series examined, with multiple peaks having $\sigma_{TPA}$ above 200 GM. The most intense absorption is predicted to occur at 597.2 nm (2.04 eV above the ground state) with a TPA cross section value of 607.5 GM (Figure 2), and populating the fifth $^1$A excited state, $6^1$A. In this instance NTO analysis describes the $6^1$A state as being dominated by a single configuration whose NTOs show excitation on both the phenyl and thiophene rings (Figure 3).

These electronic structure comparisons highlight what may be a formidable problem when using TPA in media used for 3D optical data storage, namely, that alternative reaction pathways based upon excitation of the C−C skeletal periphery may compete with the desired photoisomerization process. This would lead to alternative photochemical products that exhibit

different thermal and photochemical properties relative to the isomerization product. In turn, the media would have decreased resistance to nonlinear optical photofatigue, minimizing the applicability of such photochromophores as media for multiple read−write information storage devices.

The potential for alternative reaction mechanisms will be dependent upon the lifetime of the two-photon absorbing state. A large Franck−Condon factor, coupled with high activation barriers along the TPA excited state potential energy surface, would lead to rapid decay from the two-photon absorbing state to a lower energy state that may lead to the desired isomerization product. However, a small activation barrier along the two-photon state potential surface, coupled with a long excited state lifetime, increases the viability of observing alternative photochemical products. To address this issue, our group is currently mapping out the potential energy surfaces of the excited states relevant to two-photon absorption.

## Conclusions

Prompted by their relevance as potential candidates for 3D optical data storage media, we have examined the linear and nonlinear optical properties of photochromophores **1**−**3** using TDDFT. Within this theme, the two-photon absorption properties of each isomeric form, in addition to the electronic structure of the excited states populated by TPA, are particularly relevant. While OPA is known to lead to photoisomerization between the open- and closed-ring forms of **1**−**3**, it remains to be seen whether the TPA populated excited states are the same as those excited by linear absorption, and whether TPA will induce similar reactivity. The TDDFT results from this study clearly show alteration of the one-photon absorption as a function of isomer, with shifts of up to 200 nm for the lowest energy transition. The TPA properties exhibit a stronger dependence upon the isomeric form, with *complete* photoswitching of the nonlinear response being observed in **2** and **3** (i.e., one isomer exhibits TPA while the second isomer has no nonlinear optical response). This observation emphasizes the vast synthetic tunability of two-photon absorption in general and indicates the need for a more comprehensive understanding of the electronic features that contribute to the magnitude of the second-order nonlinear optical behavior. More importantly, it is found that the excited states populated by two-photon absorption are much higher in energy than the low-energy states with significant oscillator strength in the linear regime. A detailed comparison of the natural transition orbitals associated with TPA and OPA states reveals that both excitations are $\pi\pi^*$ in character. However, while the lowest energy OPA leads to population of $\pi\pi^*$ excited states associated with the C−C skeletal core involved in photoisomerization, TPA leads to $\pi\pi^*$ excitation along the outer C−C framework associated with the phenyl periphery. In the case of *cis*-stilbene, the lowest energy one-photon absorption populates the $1^1$B state, which is essentially a $\pi\pi^*$ excitation of the bridging ethyl unit. The lowest energy two-photon absorbing state, $2^1$A, lies 1 eV higher in energy than the $1^1$B and involves $\pi\pi^*$ excitation on the phenyl rings, with no appreciable excitation on the bridging ethyl moiety. Similar results are obtained for the remaining photochromophores examined. As a result, it possible that TPA will lead to alternative photochemical pathways to photoisomerization about the central C−C bond. This study illustrates the need for detailed theoretical examination of the potential energy surfaces associated with reactivity induced by two-photon absorption (currently in progress), in addition to experimental studies of the product distributions that result from such excitations.

**Acknowledgment.** This work was supported by a Directors Fellowship at Los Alamos National Laboratory in addition to startup funds provided by Washington State University. A.E.C. thanks Sergei Tretiak for his thoughtful comments.

**Supporting Information Available:** Table 1S containing calculated structural parameters for **1a**,**b**, **2a**,**b**, and **3a**,**b**. This material is available free of charge via the Internet at http://pubs.acs.org.

## References and Notes

(1) Tamai, N.; Miyasaka, H. *Chem. Rev.* **2000**, *100*, 1875.
(2) Tamai, N.; Saika, T.; Shimidzu, T.; Irie, M. *J. Phys. Chem.* **1996**, *100*, 4689.
(3) Miyasaka, H.; Araki, S.; Tabata, A.; Nobuto, T.; Malaga, N.; Irie, M. *Chem. Phys. Lett.* **1994**, *230*, 249.
(4) Miyasaka, H.; Nobuto, T.; Itaya, A.; Tamai, N.; Irie, M. *Chem. Phys. Lett.* **1997**, *269*, 281.
(5) Kobatake, S.; Shibata, K.; Uchida, K.; Irie, M. *J. Am. Chem. Soc* **2000**, *122*, 12135.
(6) Ern, J.; Bens, A. T.; Martin, H.-D.; Mukamel, S.; Schmid, D.; Tretiak, S.; Tsiper, E.; Kryschi, C. *Chem. Phys.* **1999**, *246*, 115.
(7) Ern, J.; Bens, A.; Martin, H.-D.; Mukamel, S.; Schmid, D.; Tretiak, S.; Tsiper, E.; Kryschi, C. *J. Lumin.* **2000**, *87*−*88*, 742.
(8) Bens, A. T.; Frewert, D.; Kodatis, K.; Kryschi, C.; Martin, H.-D.; Trommsdorff, H. P. *Eur. J. Org. Chem.* **1998**, 2333.
(9) Kuldova, K.; Tsyganenko, K.; Corval, A.; Trommsdorff, H. P.; Bens, A. T.; Kryschi, C. *Synth. Met.* **2000**, *115*, 163.
(10) Ern, J.; Bens, A. T.; Martin, H.-D.; Mukamel, S.; Tretiak, S.; Tsyganenko, K.; Kuldova, K.; Trommsdorff, H. P.; Kryschi, C. *J. Phys. Chem.* **2001**, *105*, 1741.
(11) Irie, M. *Jpn. J. Appl. Phys.* **1989**, *28*, 215.
(12) Irie, M. *Chem. Rev.* **2000**, *100*, 1685.
(13) Tsujioka, T.; Tatezono, F.; Harada, T.; Kuroki, K.; Irie, M. *Jpn. J. Appl. Phys.* **1994**, *33*, 5788.
(14) Hamano, M.; Irie, M. *Jpn. J. Appl. Phys.* **1996**, *35*, 1764.
(15) Gilat, S. L.; Kawai, S. H.; Lehn, J.-M. *J. Chem. Soc., Chem. Commun.* **1993**, 1439.
(16) Gilat, S. L.; Kawai, S. H.; Lehn, J.-M. *Chem. Eur. J.* **1995**, *1*, 275.
(17) Tsivgoulis, G. M.; Lehn, J.-M. *Angew. Chem.* **1995**, *34*, 1119.
(18) Guillaumont, D.; Kobayashi, T.; Kanda, K.; Miyasaka, H.; Uchida, K.; Kobatake, S.; Shibata, K.; Nakamura, S.; Irie, M. *J. Phys. Chem. A* **2002**, *106*, 7222.
(19) Boggio-Pasqua, M.; Ravaglia, M.; Bearpark, M. J.; Garavelli, M.; Robb, M. A. *J. Phys. Chem. A* **2003**, *107*, 11139.
(20) Hania, P. R.; Telesca, R.; Lucas, L. N.; Pugzlys, A.; van Esch, J.; Feringa, B. L.; Snijders, J. G.; Duppen, K. *J. Phys. Chem. A* **2002**, *106*, 8498.
(21) Atassi, Y.; Delaire, J. A.; Nakatani, K. *J. Phys. Chem.* **1995**, *99*, 16320.
(22) Delaire, J. A.; Nakatani, K. *Chem. Rev.* **2000**, *100*, 1817.
(23) Tretiak, S.; Chernyak, V. *J. Chem. Phys.* **2003**, 119, 8809. Masunov, A.; Tretiak, S. *J. Phys. Chem. B* **2004**, *108*, 899. Kobko, N.; Masunov, A.; Tretiak, S. *Chem. Phys. Lett.* **2004**, *392*, 444. Bartholomew, G. P.; Rumi, M.; Pond, S. J. K.; Perry, J. W.; Tretiak, S., Bazan, G. C. *J. Am. Chem. Soc.* **2004**, *126*, 11529. Katan, K. C.; Terenziani, F.; Mongin, O.; Werts, M. H. V.; Porres, L.; Pons, T.; Mertz, J.; Tretiak, S.; Blanchard-Desce, M. *J. Phys. Chem. A* **2005**, *109*, 3024. Badaeva, E. A.; Timofeeva, T. V.; Masunov, A.; Tretiak, S. *J. Phys. Chem. A* **2005**, *109*, 7276.
(24) Lee, C.; Yang, W.; Parr, R. G. *Phys. Rev. B* **1988**, *37*, 785.
(25) Becke, A. D. *Phys. Rev. A* **1988**, *38*, 3098.
(26) Rassalov, V. A.; Pople, J. A.; Ratner, M.; Windus, T. L. *J. Chem. Phys.* **1998**, *109*, 1223.
(27) Harihan, P. C.; Pople, J. A. *Theor. Chim. Acta* **1973**, *28*, 213.
(28) Francl, M. M.; Pietro, W. J.; Hehre, W. J.; Binkley, J. S.; Gordon, M. S.; DeFree, D. J.; Pople, J. A. *J. Chem. Phys.* **1982**, *77*, 3654.
(29) Frisch, M. J.; Trucks, G. W.; Schlegel, H. B.; Scuseria, G. E.; Robb, M. A.; Cheeseman, J. R.; Montgomery, J. A., Jr.; Vreven, T.; Kudin, K. N.; Burant, J. C.; Millam, J. M.; Iyengar, S. S.; Tomasi, J.; Barone, V.; Mennucci, B.; Cossi, M.; Scalmani, G.; Rega, N.; Petersson, G. A.; Nakatsuji, H.; Hada, M.; Ehara, M.; Toyota, K.; Fukuda, R.; Hasegawa, J.; Ishida, M.; Nakajima, T.; Honda, Y.; Kitao, O.; Nakai, H.; Klene, M.; Li, X.; Knox, J. E.; Hratchian, H. P.; Cross, J. B.; Bakken, V.; Adamo, C.; Jaramillo, J.; Gomperts, R.; Stratmann, R. E.; Yazyev, O.; Austin, A. J.; Cammi, R.; Pomelli, C.; Ochterski, J. W.; Ayala, P. Y.; Morokuma, K.; Voth, G. A.; Salvador, P.; Dannenberg, J. J.; Zakrzewski, V. G.; Dapprich, S.; Daniels, A. D.; Strain, M. C.; Farkas, O.; Malick, D. K.; Rabuck, A. D.; Raghavachari, K.; Foresman, J. B.; Ortiz, J. V.; Cui, Q.; Baboul, A. G.; Clifford, S.; Cioslowski, J.; Stefanov, B. B.; Liu, G.; Liashenko, A.;

Piskorz, P.; Komaromi, I.; Martin, R. L.; Fox, D. J.; Keith, T.; Al-Laham, M. A.; Peng, C. Y.; Nanayakkara, A.; Challacombe, M.; Gill, P. M. W.; Johnson, B.; Chen, W.; Wong, M. W.; Gonzalez, C.; Pople, J. A. *Gaussian03 Rev C.01*; Gaussian, Inc.: Pittsburgh, 2003.

(30) Batista, E. R.; Martin, R. L. *Encyclopedia of Computational Chemistry*; John Wiley and Sons Ltd.: Chichester, U.K., 2003.

(31) Martin, R. L. *J. Chem. Phys.* **2003**, *118*, 4775.

(32) Frisch, M. J.; Trucks, G. W.; Schlegel, H. B.; Scuseria, G. E.; Robb, M. A.; Cheeseman, J. R.; Zakrzewski, V. G.; Montgomery, J. A., Jr.; Stratmann, R. E.; Burant, J. C.; Dapprich, S.; Millam, J. M.; Daniels, A. D.; Kudin, K. N.; Strain, M. C.; Farkas, O.; Tomasi, J.; Barone, V.; Cossi, M.; Cammi, R.; Mennucci, B.; Pomelli, C.; Adamo, C.; Clifford, S.; Ochterski, J.; Petersson, G. A.; Ayala, P. Y.; Cui, Q.; Morokuma, K.; Malick, D. K.; Rabuck, A. D.; Raghavachari, K.; Foresman, J. B.; Cioslowski, J.; Ortiz, J. V.; Stefanov, B. B.; Liu, G.; Liashenko, A.; Piskorz, P.; Komaromi, I.; Gomperts, R.; Martin, R. L.; Fox, D. J.; Keith, T.; Al-Laham, M. A.; Peng, C. Y.; Nanayakkara, A.; Gonzalez, C.; Challacombe, M.; Gill, P. M. W.; Johnson, B.; Chen, W.; Wong, M. W.; Andres, J. L.; Gonzalez, C.; Head-Gordon, M.; Replogle, E. S.; Pople, J. A. *Gaussian Rev. A.7*, A.7 ed.; Gaussian, Inc.: Pittsburgh, PA, 1998.

(33) Quenneville, J.; Martinez, T. J. *J. Phys. Chem. A* **2003**, *107*, 829.

(34) Muszkat, K. A.; Eisenstein, M.; Fischer, E.; Wagner, A.; Ittah, Y.; Luttke, W. *J. Am. Chem. Soc.* **1997**, *119*, 9351.

(35) Cosmo, R.; Hambley, T. W.; Sternhell, S. *J. Org. Chem.* **1987**, *52*, 3119.

(36) Nakamura, S.; Irie, M. *J. Org. Chem.* **1988**, *53*, 6136.

(37) Moore, W. M.; Morgan, D. D.; Stermitz, F. R. *J. Am. Chem. Soc.* **1963**, *85*, 829.

(38) Muszkat, K. A.; Fischer, E. *J. Chem. Soc. B* **1967**, 662.

(39) Williams, R. V.; Edwards, W. D.; Vij, A.; Mitchell, R. H. *J. Org. Chem.* **1998**, *63*, 3125.

(40) Blattman, H. R.; Schmidt, W. *Tetrahedron* **1970**, *26*, 5885.

(41) Blattmann, H.-R.; Meuche, D.; Heilbronner, E.; Molyneux, R. J.; Boekelheide, V. *J. Am. Chem. Soc.* **1965**, *87*, 130.

(42) Huelmo, J. M. H.; Garcia, M. J. R. *J. Mol. Struct. (THEOCHEM)* **1992**, *257*, 279.

(43) Mitchell, R. H.; Iyer, V. S.; Mahandevan, R.; Venugopalan, S.; Zhou, P. *J. Org. Chem.* **1996**, *61*, 5116.

(44) Matsuda, K.; Irie, M. *Chem. Lett.* **2000**, 16.

(45) Matsuda, K.; Irie, M. *J. Am. Chem. Soc* **2000**, *122*, 7195.

(46) Yokoyama, Y.; Shirishi, H.; Tani, Y.; Yokoyama, Y.; Yamaguchi, Y. *J. Am. Chem. Soc.* **2003**, *125*, 7194.